

EVALUATION OF THE FLOW IN AN INTERMEDIATE TURBINE DUCT AT OFF-DESIGN CONDITIONS

Lars-Uno Axelsson, T. Gunnar Johansson
Chalmers University of Technology

Keywords: *Intermediate turbine duct, pressure measurements, off-design performance*

Abstract

Intermediate turbine ducts are used in modern turbofan engines for connecting the high-pressure turbine with the low-pressure turbine. The demands for engines with higher by-pass ratios require these ducts to be more "aggressive", i.e., to have a larger radial off-set and to be shorter. However, the flow in the intermediate turbine ducts are complex and therefore difficult to predict. Therefore a better understanding of the flow physics is necessary and measurements for CFD validation are needed.

This paper presents time-averaged measurements of the flow in a state-at-the-art intermediate turbine duct with an upstream high-pressure turbine present. The investigation focuses on the intermediate turbine duct flow field development for different turbine conditions. The measurements consist of area traverses with a five-hole pressure probe at different axial locations within the intermediate turbine duct. In addition, a discussion of the endwall static pressure distribution and the overall pressure losses for the different conditions are done.

Nomenclature

A_{in}	ITD inlet area
A_{out}	ITD outlet area
C_p	Static pressure coeff. = $(P_{s,i} - \overline{P_{s,C}}) / (\overline{P_{t,C}} - \overline{P_{s,C}})$
$C_{p,t}$	Total pressure coeff. = $P_{t,i} / \overline{P_{t,C}}$
L	ITD axial length
P_t	Total pressure
P_s	Static pressure

U_x	Axial velocity
U_r	Radial velocity
U_θ	Tangential velocity

Greek

α	Swirl angle
β	Radial angle
Δh_{in}	ITD inlet channel height
Δr_m	ITD mean line radius change
ξ	Pressure loss coeff. = $(\overline{P_{t,i}} - \overline{P_{t,C}}) / (\overline{P_{t,C}} - \overline{P_{s,C}})$
φ	Turbine flow coefficient
ψ	Turbine loading coefficient

Acronyms

AIDA	Aggressive intermediate duct aerodynamics
ITD	Intermediate turbine duct
HPT	High-pressure turbine
LPT	Low-pressure turbine
NGV	Nozzle guide vane

Superscripts and subscripts

—	Area averaged quantity
C	Plane C
i	Local position or plane index (C, C3, D and F)

1 Introduction

The demands for more efficient and environmentally friendly jet engines require the future turbofan engines to have larger by-pass ratios. This leads to that the radial off-set between the high-pressure turbine (HPT) and low-pressure turbine (LPT) increases; hence, the radial off-set of the intermediate turbine duct (ITD) connecting the HPT to the LPT also increases. In order to reduce the engine weight the ITDs are preferable shortened but this increases the potential risk of endwall flow separation. Even without the presence of a flow separation the flow in the ITDs is complex with, for example, rotating wakes and hub and tip vortices coming from the upstream HPT. This complicates the prediction of the flow and a good insight into the flow physics and suitable data that could be used for CFD validation are needed.

As part of an attempt to increase the knowledge regarding ITD flows the EU FP6 project AIDA (Aggressive intermediate duct aerodynamics for competitive and environmentally friendly jet engines) was initiated. As part of this project a large-scale, low-speed, turbine facility was designed and implemented at Chalmers University of technology and a detailed measurement campaign of the flow field development in a state-of-the-art ITD is being carried out. The time-averaged mean flow field and turbulence development for the nominal HPT design condition has been presented in [1]. However, it is also of interest to see how the ITD flow is affected when running the HPT at off-design conditions. A first analysis of the off-design performance was given in [2] and the results showed that no flow separation could be detected on the hub and shroud endwalls for neither the design condition nor the off-design conditions. This paper extends that analysis by looking at the mean flow field development throughout the ITD for the off-design conditions and with comparison to the design point.

Table 1 Characteristics of the HPT and ITD.

HPT	
No. vanes	36
No. blades	72
Nominal mass flow [kg/s]	9.4
Tip gap [%]	1.5
ITD	
No. vanes	72
Area ratio ($\frac{A_{out}}{A_{in}}$) [-]	1.3
Non-dimensional radial change ($\frac{\Delta r_{in}}{L}$) [-]	2.0
Non-dimensional length ($\frac{\Delta l_{in}}{L}$) [-]	0.58

2 Experimental set-up

The large-scale, low-speed, experimental turbine facility used in the present investigation is designed as a closed-loop wind tunnel. The air flow is provided by a centrifugal fan powered by a 110 kW electrical motor. The air flow is led through a wide-angle diffuser and a 90° corner with guide vanes before the flow enters a flow conditioning section. After the flow conditioning unit a nose cone is located which transforms the flow in to an annular flow. Four circumferential equally spaced thick struts are used to provide structural support to the center-body. In order to reduce the effect of the vane wakes a screen is located downstream. Next, the single-stage turbine (36 stator vanes and 72 rotor blades) used for reproducing realistic inlet boundary conditions to the ITD is located downstream the last screen. The vane and blade counts is chosen to simplify numerical computations. The ITD is located immediately behind the HPT. Its aero-design has been by Industria de Turbo Propulsores and it has been designed to be aggressive but without any endwall flow separation. Its length is about 20% shorter than a corresponding current ITD in use. The ITD includes 72 co-rotating vanes corresponding to the first vane row of a downstream LPT stage. The design of the ITD is presented in [2]. A schematic of the HPT and ITD sections can be seen in figure 1. After the ITD an annular section

EVALUATION OF THE FLOW IN AN INTERMEDIATE TURBINE DUCT AT OFF-DESIGN CONDITIONS

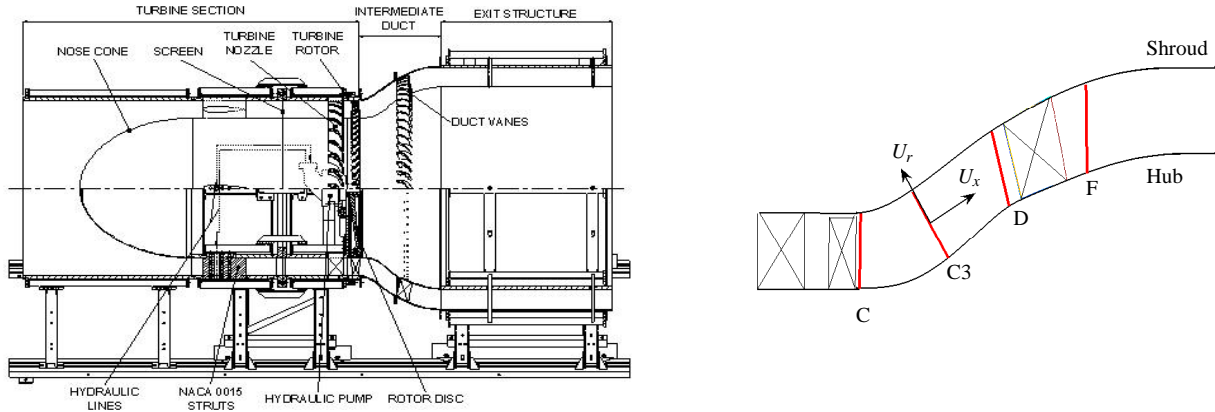


Fig. 1 Close-up of the HPT and ITD sections of the Chalmers large-scale facility showing the measurement planes and coordinate system.

used for providing mechanical support to the ITD is located. The annular section exhausts the air to the surroundings before it is sucked back into a return channel and led back to the fan. The return channel houses two radiators that are used to keep the air flow temperature constant to within $\pm 0.5^\circ$. A selection of the most important characteristics of the HPT and ITD are given in Table 1 and more details of the facility can be found in [3], [4] and [5].

Area traverses using a five-hole pressure probe have been carried out at 9 axial locations within the ITD. In the present paper results from 4 of the locations (as indicated in figure 1) will be discussed. The first plane (C) is located immediately downstream the HPT, the second plane (C3) is about half way through the duct, the third plane (D) is located upstream the LPT vanes and the last plane (F) is located downstream the LPT vanes where a corresponding LPT rotor blade row would be placed. The axial (U_x) and radial (U_r) velocity components are perpendicular and parallel to the local measurement plane, respectively. The tangential velocity (U_θ) is positive in the turbine rotational direction. The radial (β) and swirl (α) angles are defined as the angle between U_r-U_x and $U_\theta-U_x$, respectively. The area traverses performed cover a 10° sector which equals one HPT vane pitch. The five-hole probe has a conical tip head of 1.6 mm in diameter manufactured by AeroProbe Corporation Inc.

Table 2 Characteristics for the 3 different cases.

	Case A	Case B	Case C
Re	170 000	170 000	170 000
$\bar{\alpha}_c$	-16.4	-25.7	-8.7
ψ	1.1	1.4	0.97
ϕ	0.42	0.47	0.39

The five pressure holes is connected to a PSI9116 pressure scanner. For the endwall static pressure distributions on the hub and shroud some 600 pressure taps were used. The pressure taps were connected to a Scanivale multiplexer unit and the measurements were acquired with the PSI9116 pressure system.

Two off-design conditions are measured and compared to the nominal design point. The Reynolds number, based on the axial velocity and the ITD inlet channel height, is kept constant for three cases. The swirl angle (α) is changed for the three cases by changing the turbine loading. The characteristics for the three test cases are given in Table 2. Case A is the the nominal design point, Case B has larger turbine load and flow coefficients producing a larger swirl angle and Case C has lower turbine load and flow coefficients leading to a reduced swirl angle.

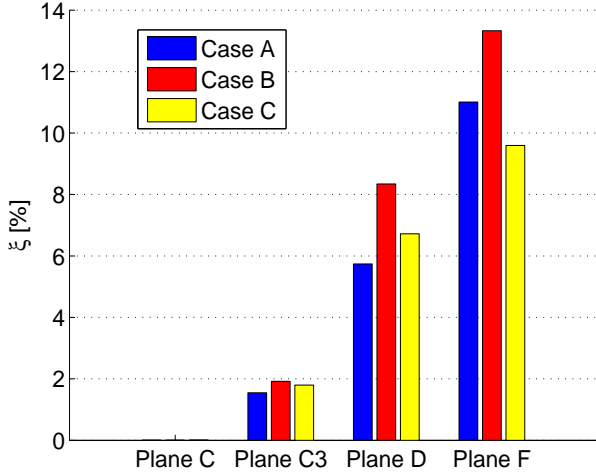


Fig. 2 Pressure loss coefficient distribution for the different cases.

3 Results

This section compares the results for the three cases starting by looking at the overall performance (i.e., pressure loss distribution) and the endwall static pressure distribution. This part is followed by a more detailed analysis of the time-averaged mean flow field development throughout the ITD.

3.1 Pressure losses and endwall static pressure distribution

We start by looking how the pressure losses are changing as the flow proceeds downstream for the three cases. In figure 2 the pressure loss coefficients for each of the evaluated measurement planes are shown. The pressure loss coefficient is defined as:

$$\xi = \frac{\overline{P_{t,i}} - \overline{P_{t,C}}}{\overline{P_{t,C}} - \overline{P_{s,C}}} \quad (1)$$

where $\overline{P_{t,i}}$ is the area-averaged total pressure at the different planes, $\overline{P_{t,1}}$ is the area-averaged total pressure at plane C and $\overline{P_{s,c}}$ is the area-averaged static pressure at plane C. At plane C3 the pressure loss coefficients are about the same and fairly small for three cases, which is expected since it is mostly the friction losses that have pro-

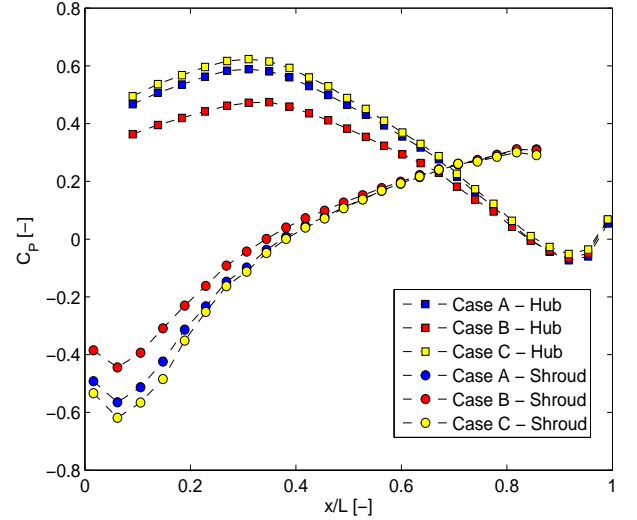


Fig. 3 Circumferential averaged static pressure coefficient distribution along the ITD endwalls.

duced the losses up to this stage. Before the LPT vanes, plane D, the pressure losses has increased to just below 6% for case A and to slightly more than 8% for case B. Case C has slightly more losses here but one should note that the differences between cases A and C are within the uncertainty range for the pressure measurements. The reason the losses are higher for case B might be explained by the fact that the fluid particles have travelled a longer distance for this case compared to the other; hence, the frictions losses are larger. Downstream the vane the largest loss occur for case B which are now almost 14% of the inlet dynamic head. Interestingly, the lowest pressure loss (<10%) is for case C and not for the design point. This might partly be explained with that less turning is required for case C as the flow passes through the LPT vanes. However, it is expected that an even lower load of the turbine would cause the flow to separate on the LPT vanes and then the losses would increase.

Besides the pressure loss distributions, the static pressure distributions along the endwall give an insight to the performance of the ITD. In figure 3 the circumferential averaged endwall static pressure distributions between the HPT and LPT vanes are shown. The peak pressure occurs in the first bend on the hub. The case with

EVALUATION OF THE FLOW IN AN INTERMEDIATE TURBINE DUCT AT OFF-DESIGN CONDITIONS

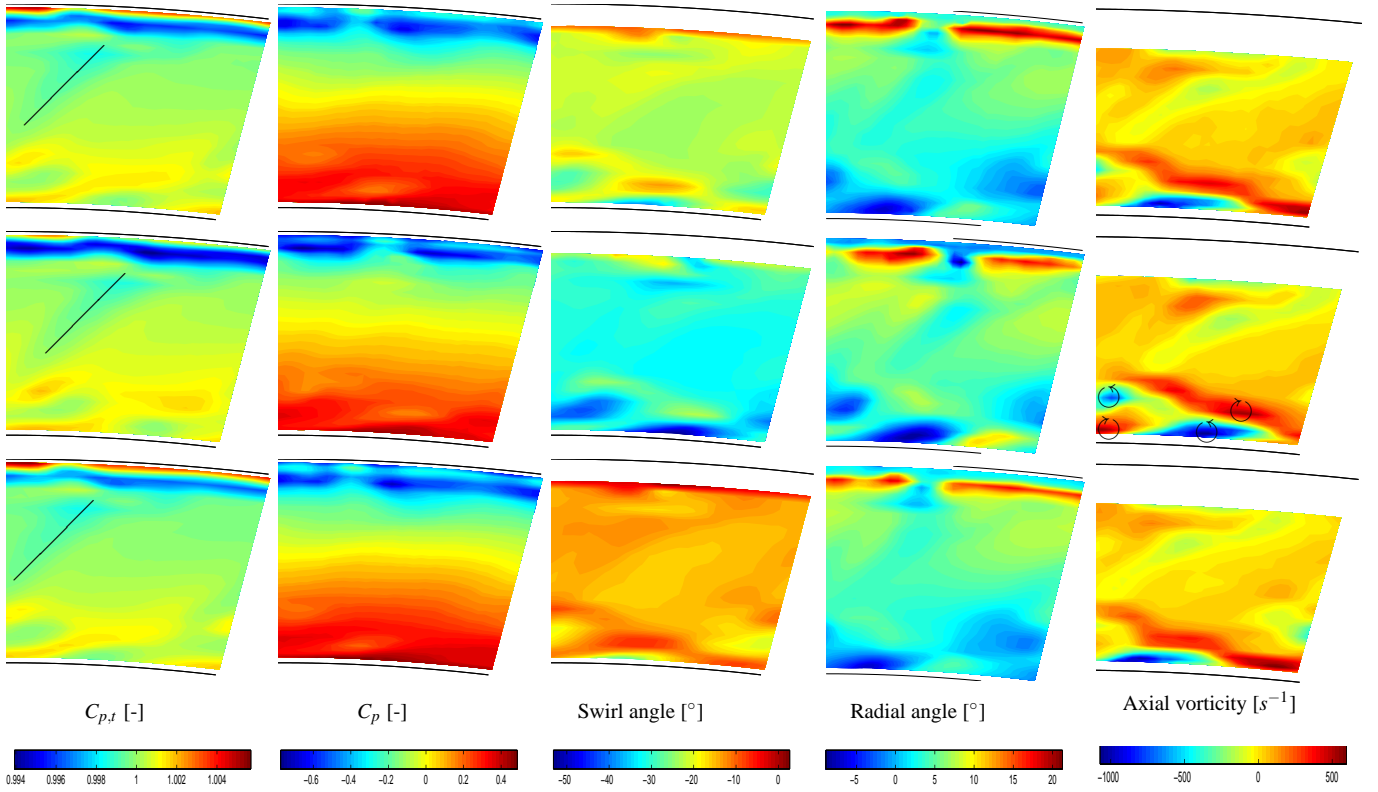


Fig. 4 5-hole probe results for plane C. Top row: Case A; Middle row: Case B; Bottom row: Case C.

the shortest flow path, case C, experiences the largest pressure peak. This has been observed in previous ITD investigations, e.g., [6]. As the flow proceeds to the LPT vanes the pressure decreases along the hub due to the acceleration of the flow. As the flow approaches LPT vanes the static pressure evens out between the three different cases; hence, the static pressure has to decrease more rapidly for case C. Looking at the shroud (right column) one can note that the lowest pressure occur in the first bend and therefore the radial pressure gradient between the hub and shroud is largest in the first bend. In the same way as for the hub, the pressure evens out as the flow proceeds towards the LPT vanes since the flow decelerates after the first bend. The adverse pressure gradient that occurs on the shroud creates a potential risk of flow separation; hence, the largest risk should occur for case C since the static pressure increases more rapidly for this case as the flow proceeds downstream. However, no flow separation could be detected from the oil-film flow visualization carried out in the earlier investigation and reported in [2].

3.2 Mean flow field development

In order to characterize the differences in the development of the flow field for the three cases the time-averaged results from the five-hole probe are analyzed for each of the four axial locations. In figure 4 the results from area traverses at the inlet plane, **plane C**, are shown. The contour plots show from left to right: Total pressure coefficient, static pressure coefficient, swirl angle, radial angle and mean axial vorticity. The top row represents case A, the middle row case B and the bottom row case C. This structure will be used throughout this section unless otherwise stated.

Three major features dominate the flow structure at the first plane: The upstream HPT vane wake (indicated by black lines), the tip leakage region and the hub vortices. The first thing to notice is that the total pressure is higher in the major part of region outside HPT vane wake for higher loading while the opposite occurs in the tip leakage region. When the flow angle increases the velocity magnitude increases (remember that the axial velocity is kept constant for all cases)

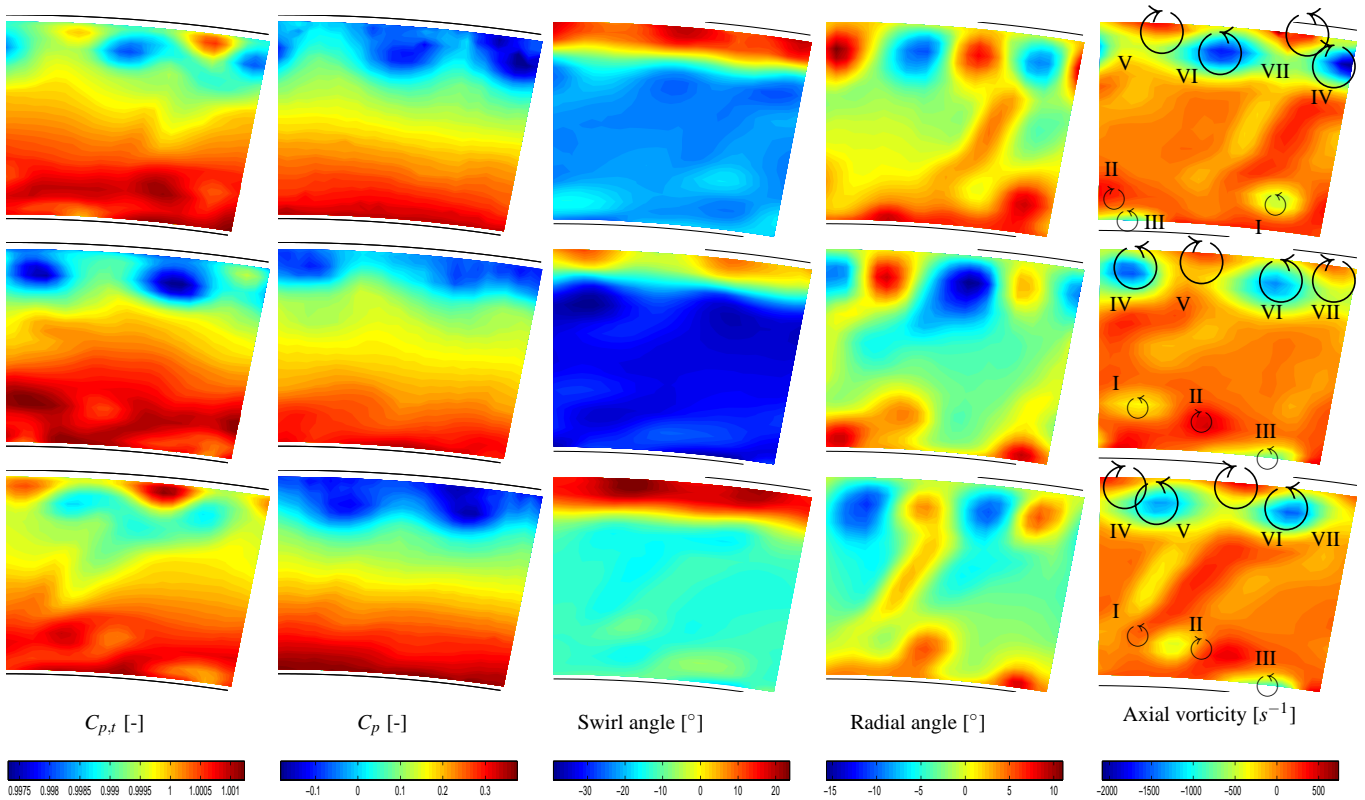


Fig. 5 5-hole probe results for plane C3. Top row: Case A; Middle row: Case B; Bottom row: Case C.

and hence there is a subsequent reduction of the static pressure in order to accomplish the larger flow turning. The first duct bend is felt already at the inlet plane and therefore the static pressure is increasing from the hub to the shroud for all cases. This can also be seen from the radial angle where the pressure gradient creates a radial flow upwards.

The tip leakage region dominates the flow at the inlet plane which result in a vorticity region with high strength. In order to reveal the vortical structures within the major part of the flow the measurement points closest to the shroud is omitted from the figures for the streamwise vorticity. The hub vortices (indicated by arrows for case B) are dominates the region closest to the hub for all three cases. Note that negative and positive vorticity indicate counter-clockwise and clockwise rotation, respectively. No major differences are seen between the three cases in terms of the overall vortical structures present but the size of the vortices differ. The region of negative vorticity closest to the hub is more compressed in the radial direction as the swirl angle

decreases. The other region of negative vorticity has a similar shape for the different cases but the region becomes larger in extent as the swirl angle increases. There are also regions of positive vorticity close to the hub. The regions of positive/negative vorticity modifies the swirl angle in these regions, i.e., the regions of negative vorticity cause an overturning of the flow while the positive regions cause overturning which can be seen in clearly in the contour plots of the swirl angles (positive swirl angle is flow going to the left). As for the vorticity plots the measurement points closest to the shroud have been excluded in order to reveal more details of the swirl angles.

As the flow proceeds downstream (**plane C3**) the tip shear-layer has started to break up and two pairs of counter-rotating vortices (IV-V and VI-VII) occupy about 25% of the channel height as can be seen in figure 5. One can see that the two clockwise rotating vortices have started a pairing process. These vortices create a non-uniformity within the tip leakage where the swirl angles are clearly affected. As the turbine load is increased the pairing process is stronger. This could be an

EVALUATION OF THE FLOW IN AN INTERMEDIATE TURBINE DUCT AT OFF-DESIGN CONDITIONS

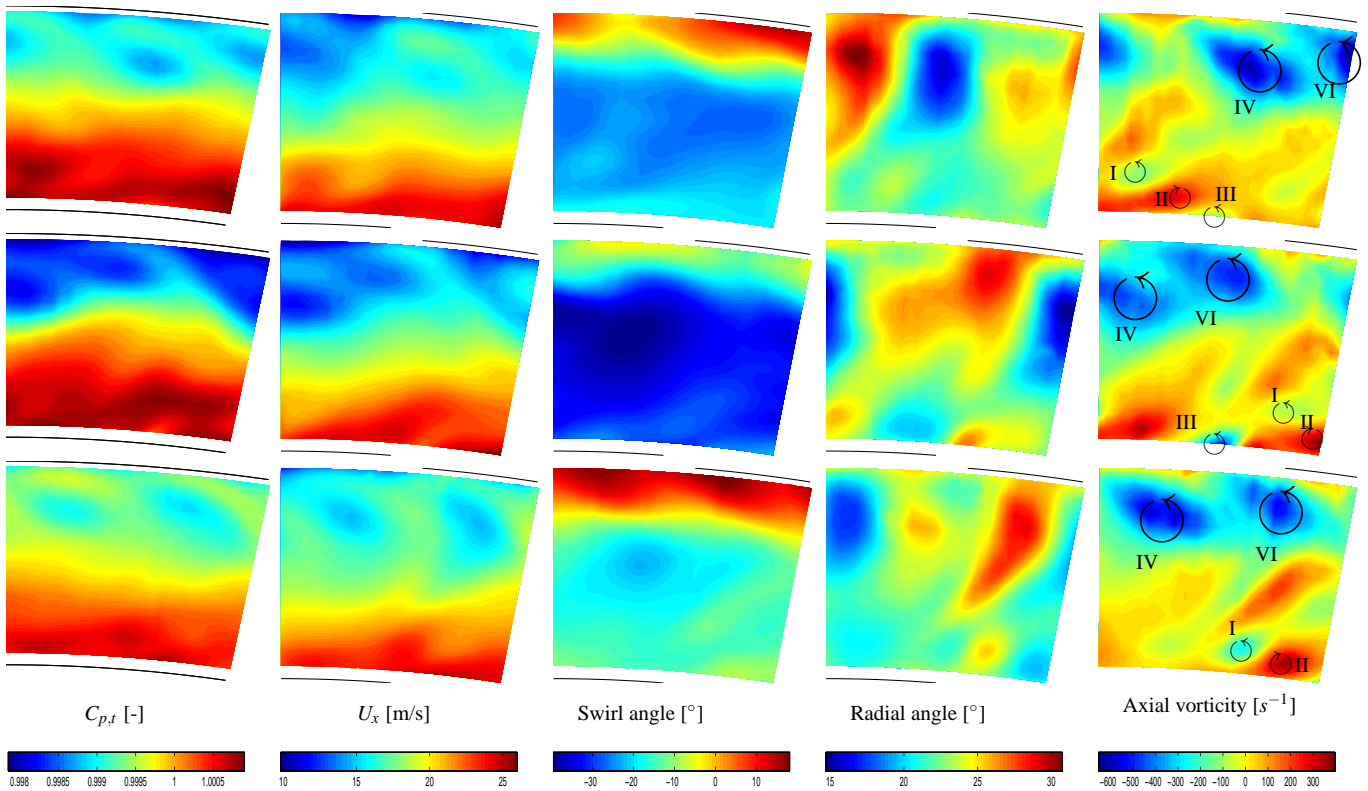


Fig. 6 5-hole probe results for plane D. Top row: Case A; Middle row: Case B; Bottom row: Case C.

effect of the fact that the fluid particles have travelled a longer distance for case B and therefore this process has evolved more for this case. The merging of vortices in swirling ITD flows was also observed in the investigation by [6].

The wake from the upstream HPT vane are still clearly visible but the wakes are getting more pronounced as the turbine loading decreases causing a larger pressure loss region. In addition, there are two low-pressure regions associated with the counter-clockwise rotating vortices at the shroud, which are larger and with a lower axial speed for case B while Case C shows much smaller regions. This reduction of axial velocity together with a reduction in swirl angle in the tip region leads to that the pressure losses are larger for case B. This increases the pressure loss coefficient shown in figure 2 which is highest for case B at plane C3. Close to the hub the three vortices that were seen at the inlet plane are still present. The counter-clockwise (III) and clockwise (II) rotating vortices closest to the hub are similar for the three cases but the counter-clockwise rotating vortex (I) located fur-

ther away from the wall and next to the HPT vane wake differs in size and strength. As the turbine loading increases this vortex is flattened and strength is reduced. This could, as mentioned before, be due to that the flow has travelled a longer distance for case B and hence the vortex strength has decreased. The change in shape could be due to that the flow is not approaching the measurement plane perpendicular to it and as the swirl angle increases the vortices will appear more oval shaped. However, this is not seen for the other vortices which would be the case if this would be the only explanation for the difference in shape. The hub vortices modifies the radial and swirl angles locally. Vortices I and II causes a stronger radial flow upwards when both their directions are upwards and subsequently a downwards flow when both their directions are pointing downwards. The interaction between the vortices II and III next to the hub modify the swirl angle in this region making it less negative. The vortices closest to the wake (I and II) are producing an overturning close to the hub followed by an under-turning further away

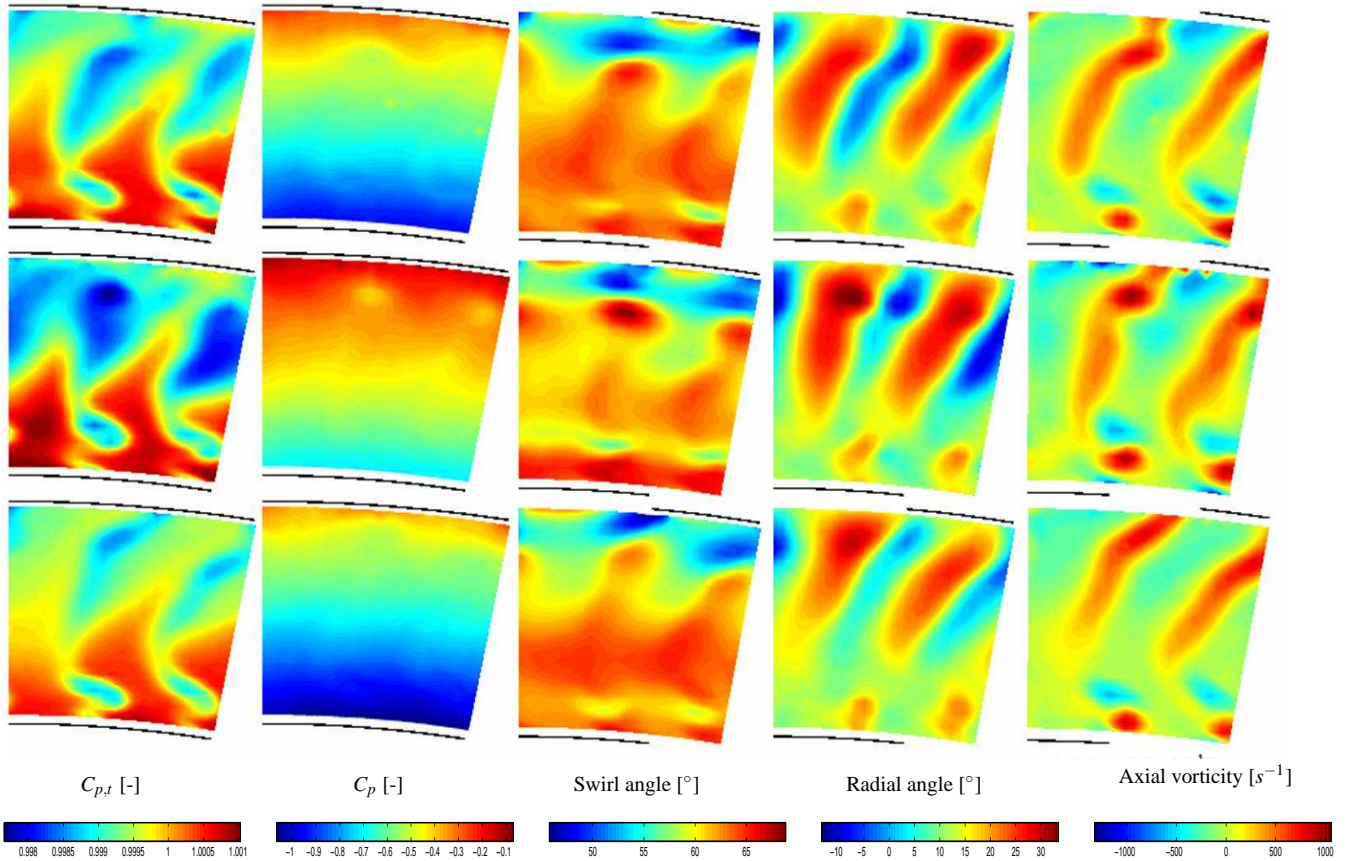


Fig. 7 5-hole probe results for plane F. Top row: Case A; Middle row: Case B; Bottom row: Case C.

from the wall. Another interesting fact is that the HPT vane wake and shroud vortices are moving at different speeds relative each other. This can be seen in the contour plots of radial angle where the HPT wake for case C interacts with one of the regions of positive radial angle while for case B the wake interacts with a region of negative radial angle.

The effect of different HPT loading on the downstream LPT vanes is crucial for their performance. Figure 6 shows the measurements as the flow is about to enter the LPT vane row, **plane D**. The two counter-clockwise rotating vortices (IV and VI) emanating from the tip leakage has now grown in size but they have also decreased in strength. The interaction of the two vortices that were seen at plane C3 has continued and they have almost merged together at this stage. These vortices create regions with lower total pressure and they have at this stage about the same size and strength for the three cases.

The potential field created in the vicinity of the leading edges of the LPT vanes are clearly visible in the axial velocity as the velocity decreases there (remember that the the HPT-to-LPT-vane count is 1:2). At this location, the tip vortices dominate both the radial and swirl angle distributions. For case B the downstream LPT vane is expected to increase the pressure loss since the flow has to be turned more in this case. Less work is expected to be done for case C and this might be one reason for the lower loss that is seen downstream the LPT vanes in figure 2. The swirl angles differ by some 20° for the three cases and the vanes need to be able to handle these variations. The hub vortices (I and II) are locked to the position of the HPT vane wake while vortex III is located in the same positions independent of swirl angle. As the swirl angle decreases the vortex is pushed closer to the wall and for case C it is not visible at all.

It is crucial how the flow behaves downstream

the LPT vanes and especially the flow angles since they should be similar for the three cases in order to have a acceptable performance of the downstream rotor. At **plane F** the flow structure is now dominated by the two wakes from the vanes (figure 7) present in each sector. Plane F is located where a corresponding LPT rotor blade would be located; hence, this measurement plane gives an idea of how the incoming flow to the rotor would look (an incorporation of a rotor would affect the flow field at this location due to the blockage it creates). Note that the zero degree inclination of the plane leads to that the fluid at the hub has travelled a shorter distance than the fluid at the shroud.

For case B the wakes are wider and cause a larger pressure loss region, while the wakes are thinnest for case C. Note also that the wake to the left in case B is not as skewed as for the other cases and has almost merged with the neighboring wake. The axial velocity is lowest for this case with a subsequent higher static pressure. Except for the wake regions, the static pressure distribution has a similar pattern for the different cases. This is expected since the swirl angle out from the LPT vanes are about the same. The combination of larger turning of the flow and lower axial velocity within the wake cause a higher swirl angle in this region. For cases A and C the swirl angle shows almost the same value for most of the flow region. However, in the tip region where the wake and the endwall vortices interacts, the swirl angle differs with approximately $\pm 10^\circ$. For case C the right wake has an overturning (larger angle) compared to case A closest to the shroud followed by an underturning next below leading to fairly sharp gradients in this region. For the left wake case C shows opposite result with an underturning closest to the shroud. For case B a similar behavior is found with an overturning followed by an underturning is found for the right wake. However the magnitude for the overturning is smaller (about 5° for this case. It is worth to note that the swirl angle is larger ($2 - 5^\circ$) in the major part of the flow, especially within the left wake region.

In the hub region three vortices are found in

between each of the vane passages. The vortices are located on top of each other with counter-clockwise ones in the bottom and top. These vortices have been pushed further away from the hub for case B compared to case A, that in turn is further away than case C. The interaction between the vortices modify the swirl and radial angles with an overturning in swirl angle occur adjacent to the hub while an underturning occurs further away from the wall. However, these swirl angle differences are more pronounced for case B.

4 Conclusions

In this paper an experimental investigation of the flow field development and its implications for the performance has been presented for an intermediate turbine duct subject to different HPT loading.

From the pressure loss estimations one could see that the case with higher turbine loading (case B) produced the most losses, while the cases with nominal loading and lower loading produced similar results. For the nominal case about half of the losses occurred in the LPT vane passage while the corresponding number for the two other cases were lower.

The results from the 5-hole probe traverses showed that the formation of two large co-rotating vortices dominates the flow structure up to the LPT vanes for all three cases. These vortices seem to start a pairing process that has proceeded further for the case with higher loading (more swirl).

In spite of the fact the the swirl angles into the LPT vanes are different for different HPT loading, the angles downstream the LPT vanes are similar for most of the flow region; hence the vanes can operate under different loading and are expected to perform satisfactory. However, a slightly larger variation in swirl angles from the design case are found for case B.

Acknowledgements

This work has been carried out as part of the EU FP6 programme AIDA (Aggressive Intermediate Duct Aerodynamics for Competitive and Environmentally Friendly Jet Engines), contract no. AST3-CT-2003-502836.

References

- [1] Axelsson, L.-U., and Johansson, T. G., 2008. "Experimental investigation of the time-average flow in an intermediate turbine duct". *Proc. of ASME Turbo Expo 2008, GT2008-50829, June 9-13, Berlin, Germany*.
- [2] Axelsson, L.-U., Arroyo Osso, C., Cadrecha, D., and Johansson, T. G., 2007. "Design, performance evaluation and endwall flow structure investigation of an s-shaped intermediate turbine duct". *Proc. of ASME Turbo Expo 2007, GT2007-27650, May 14-17, Montreal, Canada*.
- [3] Arroyo, C., Axelsson, L.-U., Johansson, T. G., Håll, U., Larsson, J., and Haselbach, F., 2006. "Large-scale low-speed facility for investigation intermediate turbine flows". *Proc. 44th Aerospace Sciences Meeting and Exhibit, AIAA 2006-0873, January 9-12, Reno, Nevada, USA*.
- [4] Arroyo Osso, C., 2006. "Design of a large-scale experimental facility for the study of the flow in intermediate turbine ducts". *Licentiate thesis, Chalmers University of Technology*(Report no. 2006:08).
- [5] Axelsson, L.-U., 2006. "A large-scale facility for investigation of intermediate turbine ducts: Design, implementation and initial tests". *Licentiate thesis, Chalmers University of Technology*(Report no. 2006:12).
- [6] Dominy, R. G., and Kirkham, D. A., 1995. "The influence of swirl on the performance of inter-turbine diffusers". *VDI Berichte*(No. 1186).

Copyright Statement

The authors confirm that they, and/or their company or institution, hold copyright on all of the original material included in their paper. They also confirm they have obtained permission, from the copyright holder of any third party material included in their paper, to publish it as part of their paper. The authors grant full permission for the publication and distribution of their paper as part of the ICAS2008 proceedings or as individual off-prints from the proceedings.